International Forum on Aeroelasticity and Structural Dynamics
IFASD 2024
17-21 June 2024, The Hague, The Netherlands

EXPLAINABLE NONLINEAR STATE-SPACE MODELING: ANALYSING THE GVT OF A BATTERY-OPERATED AIRCRAFT

Péter Zoltán Csurcsia[1,2], Tim De Troyer[1,2]
[1] Thermo and Fluid Dynamics (FLOW), Faculty of Engineering, Vrije Universiteit Brussel (VUB), Pleinlaan 2, 1050, Brussels, Belgium
Brussel (VUB) and Université Libre de Bruxelles (ULB)
[2] Brussels Institute for Thermal-Fluid Systems and clean Energy (BRITE), Vrije Universiteit Brussel (VUB) and Université Libre de Bruxelles (ULB)

Keywords: Ground Vibration Testing, Flutter, Electric Aircraft, Virtual Driving Point

Abstract: Traditionally, ground vibration tests of aircraft are processed using modal analysis algorithms. Most algorithms that are in commercial use today are grounded in the domain of linear system identification. These tools have proven their worth and are still the state-of-the-art in commercial aviation, even though advances have been made in the research community. One of the more promising advances is the ability now to develop fully nonlinear models from experimental data. This capability could drastically improve the quality of information that can be extracted from a ground vibration test experiment. In this work, we utilize recently developed concepts in the nonlinear state-space modeling framework, for instance, a nonlinear state selection method for the polynomial nonlinear state-space models and nonlinear function decoupling for a state-space neural networks. These concepts enable to build more concise, nonlinear, explainable (to some extent), data-driven models. We illustrate the methodology first on an analytical example containing multiple linear modes and one isolated source of nonlinear distortion and compare the performance of classical linear techniques to the new nonlinear modeling framework. Then, we demonstrate this framework on a real-life multiple-input-multiple-output ground vibration test of the Magnus eFusion light sports aircraft.

1 INTRODUCTION

The goal of this paper is to demonstrate state-of-the-art nonlinear state-space (NSS) modeling framework to model real-life aerodynamic, aeroelastic and structural testing measurements. While we primarily focus on its application to a battery-operated small aircraft, it is important to emphasize that usage of this framework is not limited to this specific example as it can be applied to diverse applications.

Mechanical vibrating structures, such as aircrafts, often exhibit different types of nonlinear behavior. These are, for instance, free-play of control surfaces, stick-and-slip behavior at hinges, large deformations of slender wings, nonlinear friction. However, due to complexity reasons, nonlinear systems are often approximated by linear systems. This is also the case with processing

and modeling ground vibration tests (GVT): most algorithms that are in commercial use today are grounded in the domain of linear system identification.

These tools have proven their worth and are still the state-of-the-art in commercial aviation, even though advances have been made in the research community. In this work, however, instead of trying to reduce the impact of the nonlinear distortion – as common with the commercial tools – we show the potential benefit of including nonlinearities in the model structure.

When building nonlinear models from data, one of the biggest challenges is to limit the number of parameters of the model structure. This is especially true for complex nonlinear systems such as aircraft. To that end, in this work, we utilize recently developed concepts (a nonlinear state selection method, nonlinear function decoupling, a single-branch neural network) embedded in our NLSS modeling framework, to build a nonlinear, more explainable, data-driven model [1]. The key idea of the proposed framework is that we make an explicit separation between linear and nonlinear terms of the state-space models. This is beneficial because state-space models are well suited for understanding, control, and simulation.

All of the nonlinear models are initialized with the help of the so-called Best Linear Approximation (BLA) framework [2] [3] that provides the frequency response matrix (FRM) estimate and its noise and nonlinear distortion analysis. In this work, we consider two conceptually similar but technically quite different nonlinear parametric modeling approaches.

1. We extend the already existing polynomial nonlinear state-space (PNLSS) method [4] that will allow to incorporate only the state variables that are most impacted by nonlinearities in the nonlinear part of the model.

2. Furthermore, we employ nonlinear state-space neural network models (SSNN) where the nonlinear terms of the state-space models are entirely replaced by (recurrent) neural networks resulting in a much smaller number of parameters and more interpretability than using deep neural networks [5]. We also consider the decoupled model structure form with tailored – data-based - activation functions [6].

The proposed nonparametric industrial framework is illustrated on the ground vibration test (GVT) measurement of a battery-operated electrical airplane. The detailed results and modal analysis of this GVT analysis can be found in [7] [8].

The numerical results presented in this work were obtained using the SAMI (Simplified Analysis for Multiple Input Systems) toolbox. Interested readers are referred to [9]. However, our focus in this work is on the novel methodology rather than the usage of the toolbox.

This paper is organized as follows. Section 2 briefly describes the considered systems and the main assumptions applied in this work. Section 4 discusses the estimation framework. In Section 4 the description and a basic analysis of the GVT experiments are given. The modeling results are elaborated in Section 5. Conclusions can be found in Section 6.

2 BASICS

2.1 Assumptions

The considered systems are mechanical or civil dynamic vibrating structures. The linear part of the dynamics of a linear multiple-input-multiple-output (MIMO) system can be nonparametrically characterized in the frequency domain by its Frequency Response Matrix (FRM, a matrix whose elements are FRFs [10]) G at frequency bin k, which relates n_i inputs U to n_o outputs Y of N measurement samples as follows:

$$Y[k] = G[k]U[k] \tag{1}$$

where $G[k] \in \mathbb{C}^{n_o \times n_i}$, $Y[k] \in \mathbb{C}^{n_o \times 1}, U[k] \in \mathbb{C}^{n_i \times 1}$, $k = 0 \ldots \frac{N-1}{2}$ at frequency $f_k = kf_s/N$ with sampling frequency f_s.The system represented by G is linear when the superposition principle is satisfied in steady state, i.e.:

$$Y[k] = G[k]\{(a+b)U[k]\} = a\,G[k]\{U[k]\} + b\,G[k]\{U[k]\} = (a+b)\,G[k]\{U[k]\} \tag{2}$$

where a and b are scalar values. If G is constant, for any a, b (and excitation), then the system is called linear-time invariant (LTI). On the other hand, when G varies with a and b (and the variation depends also on the excitation signal – e.g. level of excitation, distribution, etc.) then the system is called nonlinear. However, if the system satisfies the principle of superposition but G varies over the measurement time, then it is known as a linear time-varying system [11].

In terms of instrumentation, it is assumed that 1) the measurement system is synchronized, 2) the excitation signal is exactly measured , 3) the actuator (e.g. shaker) of the system is nearly linear, and 4) the output is measured with time-domain additive, independent and identically distributed Gaussian noise (denoted by E) with zero mean and finite variance, such that the measurement $Y_{measured}$ is given by:

$$Y_{measured}[k] = Y[k] + E[k] \tag{3}$$

2.2 Multisine excitation and detection of nonlinearities

A wide range of excitation signals are available for efficiently and user-friendly structural testing [12]. Industrial practitioners prefer to use sine-sweep or noise excitation due to its randomness and simplicity, however, there is a potential issue with spectral leakage and limited ability to detect nonlinearities. We suggest the use of multisine signals (also known as periodic pseudo-random noise) as they are simple to create, periodic, and exhibit noise-like characteristics: in the time domain, they resemble white noise and behave similarly, although they are not actually noise [10] [13]. The magnitude characteristics of multisines are set by the user in the frequency domain (typically flat) but the phases are randomly chosen. For experiments with multiple inputs, we recommend using orthogonal multisine excitation signals [14, 15]. The proposed procedure is to generate independent random excitations for every input channel [16], as opposed to the classical Hadamard technique [17]. An illustration of the MIMO multisine signals is shown in Figure 1. Furthermore, applying multiple random realizations of the multisine signal and/or adjusting the excitation level can also make the nonlinearities more apparent. A freeware implementation of a multisine toolbox can be found in [18].

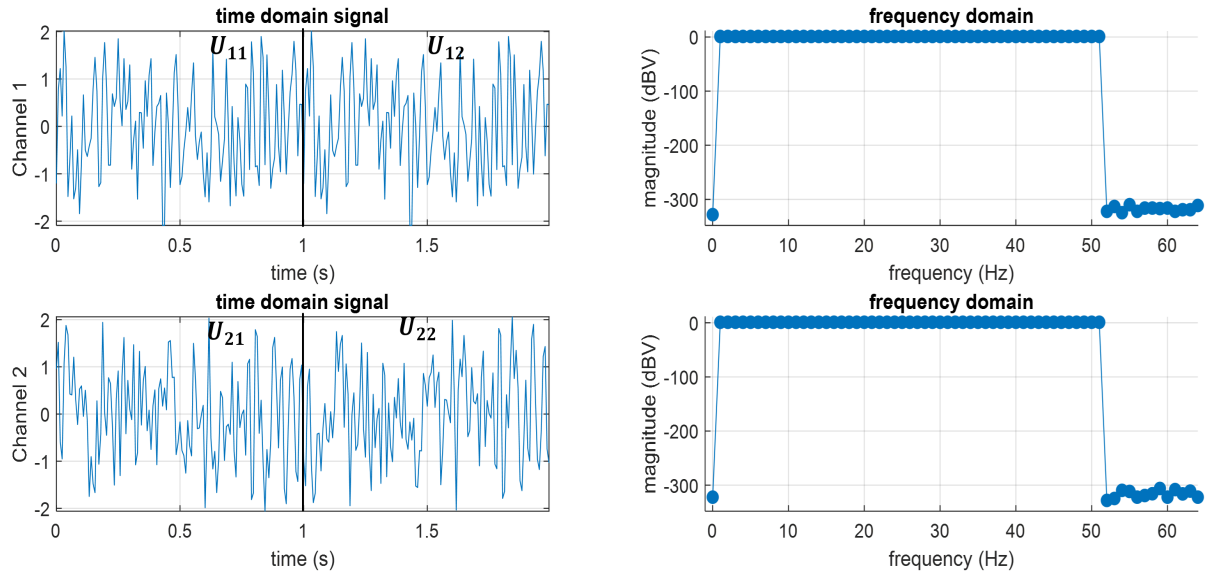

Figure 1: The proposed multisines signals for a very simple 2x2 MIMO scenario.

2.3 Best Linear Approximation models

The essence of a Best Linear Approximation (BLA) [17] is to minimize the mean squared error between the measured nonlinear response of a system and the response of a linear nonparametric frequency response function model for a given level of excitation. In the multisine-driven BLA framework, systems are excited by multiple periods and realizations of random phase multisines. The key idea is to use statistical features of the multisine excitation signal to separate the phase-coherent (linear) part of the response signal from the non-phase-coherent part (noise and nonlinear distortions), and then to reduce the random nonlinear distortions by averaging over multiple realizations of the multisine [19]. Different quantities of the BLA framework are illustrated in Figure 2. G_{linear} is the "classical" linear FRM model. The (phase non-coherent) nonlinear distortions are represented by G_s. The measurement noise is represented by the G_E. G_{Bias} represents the bias error, i.e. the remaining imperfections (e.g. additional damping introduced by shaker testing) and the coherent nonlinearities (usually it is a negligible amount of nonlinearities).

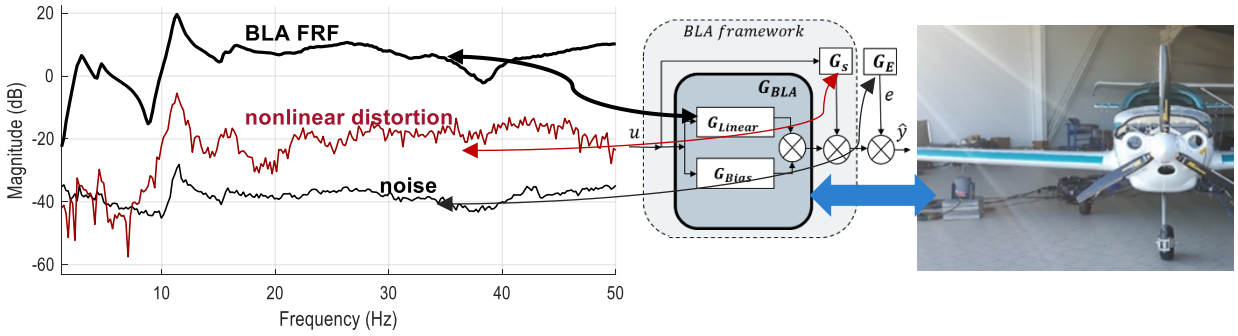

Figure 2: The theoretical structure of the best linear approximation and its connection to the FRF estimate illustrated on the transfer function estimate of a battery-operated aircraft at the driving point of the left wing.

The key idea is to use some statistical features of the excitation signal. In this framework, there are M different realizations of the multisine excitation signal, each realization is repeated P period

times. The usage of periodic excitation reduces the effects of the measurement noise (G_E). The usage of multiple realizations reduces the impact of nonlinear noise (non-coherent nonlinearities, G_s). The FRM model at period p and realization m at frequency bin k is given by:

$$\widehat{G}^{[m][p]} = \overbrace{Y^{[m][p]}_{measured} U^{[m]\dagger}}^{measured\ FRM\ at\ m,p} = (\overbrace{\widehat{G}^{[m][p]}_{BLA}}^{FRM\ estimates} + \overbrace{\widehat{G}^{[m]}_{S}}^{nonlinearity\ varies\ over\ m-\ fixed\ in\ p} + \overbrace{\widehat{G}^{[m][p]}_{E}}^{noise\ varies\ over\ p,m}) \; U^{[m]\dagger} \qquad (4)$$

where $\widehat{G}^{[m][p]} \in \mathbb{C}^{n_o \times n_i}$, $\widehat{Y}^{[m][p]}_{measured} \in \mathbb{C}^{n_o}$, $U^{[m]} \in \mathbb{C}^{n_i}$, and the † is the generalized inverse.

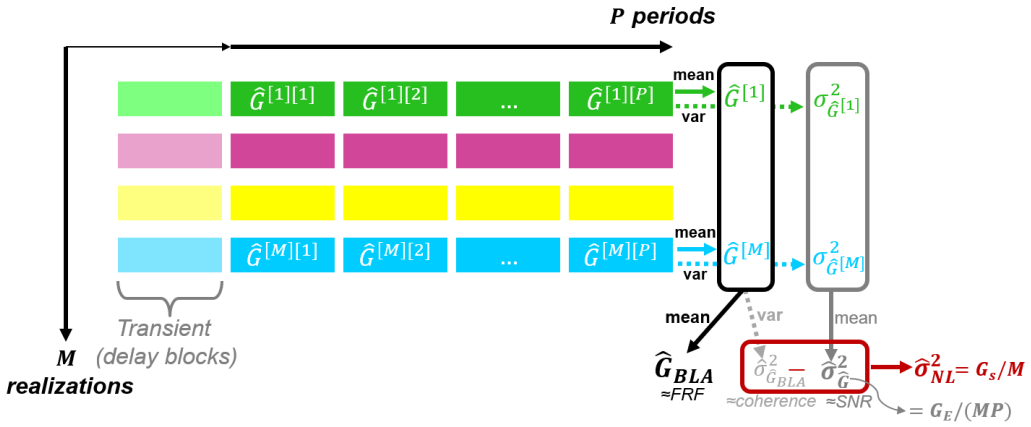

Figure 3. Evaluation of BLA estimate with the help of multidimensional averaging.

For further computational and fundamental details we refer to [17]. A freeware implementation of a BLA toolbox can be found in [20].

3 MODELING FRAMEWORK

3.1 Overview

The recommended nonlinear modeling procedure consists of the following interrelated steps:

- Step 1: Systems are excited by broadband (preferably by multisine) signals at multiple excitation levels.
- Step 2: Measurements are processed with the BLA estimation framework [17].
- Step 3: Classical linear state-space (SS) models are built based on the BLA estimates on a level closest to the linear regime of operation. The model complexity (number of states) can easily be determined with a cross-validation-based model order scanning.
- Step 4: Building nonlinear models using either polynomial or neural network basis.

Note that even though the technique works best with the recommended multisines, with some loss of useful information and accuracy any broadband signal can be applied. Next, the parametric models used in our framework will be briefly discussed.

3.2 Linear state-space models

For understanding, design and control we propose to use state-space models (in modal form). An n^{th} order discrete-time state-space model can be written as:

$$\begin{cases} x(t+1) = Ax(t) + Bu(t) \\ \quad y(t) = Cx(t) + Du(t) \end{cases} \tag{5}$$

where u and y vectors contain the input-output values at time instance t; the state vector $x \in \mathbb{R}^n$ represents the memory of the system; $A \in \mathbb{R}^{n \times n}$, $B \in \mathbb{R}^{n \times n_i}$ define the state equation; and $C \in \mathbb{R}^{n_o \times n}$, $D \in \mathbb{R}^{n_y x n_o}$ define the output equation. The state vector x includes the common dynamics present in the different outputs. The state equation represents the evolution of the state as a function of the input and the previous state. The output equation relates the system output with the state and the input. When dealing with measurements, the ideal noise free output $y(t)$ in (5) should be substituted with the experimental data $y_{measured}(t)$.

To build linear state-space models – in modal form – we use a special implementation of the SS-FRM fitting method proposed by [21]. Our experience clearly shows that this FRM based method leads to more precise models than the classical time-domain fitting SS methods like the n4sid [22]. For tunning all models (including nonlinear models) we make use of a Levenberg–Marquardt optimization routine [22].

3.3 Nonlinear State-Space models

In our framework, we make an explicit expansion of (5) to include the nonlinearities that lead to the generic nonlinear state-space form with nonlinear functions $\mathcal{E}$ and $\mathcal{F}$:

$$\begin{cases} x(t+1) = Ax(t) + Bu(t) + \mathcal{E}(x,u) \\ \quad y(t) = Cx(t) + Du(t) + \mathcal{F}(x,u) \end{cases} \tag{6}$$

Here we consider – at the moment – three different types of NSS. The first one is using polynomial basis expansion, the other two methods consider neural network expansion. In all cases, the linear parts of the NSS in (6) are initialized with the BLA SS models given in (5).

3.3.1 Polynomial Nonlinear State-Space models

3.3.1.1 Polynomial Nonlinear State-Space models

A polynomial nonlinear state-space (PNLSS) model can be expressed as:

$$\begin{cases} x(t+1) = Ax(t) + Bu(t) + E_\zeta \zeta(x,u) \\ \quad y(t) = Cx(t) + Du(t) + F_\eta \eta(x,u) \end{cases} \tag{7}$$

where $E_\zeta \in \mathbb{R}^{n x n_\zeta}$ and $F_\eta \in \mathbb{R}^{n_o x n_\eta}$. E_ζ and F_η matrices realize the nonlinear extension part where auto- and cross-terms of the input and states are considered. These terms can include, for instance, $x^2(t), u^2(t), x^2(t)u(t)$. The vectors $\zeta \in \mathbb{R}^{n_\zeta}$ and $\eta \in \mathbb{R}^{n_\eta}$ contain the nonlinear monomials in $x(t)$ and $u(t)$ of multiple chosen degrees.

The PNLSS model structure is flexible, as it can capture many different nonlinear dynamic behaviors [6]. The drawback of the method is that it even for a moderate complexity problem, there are an excessive number of model parameters needed and it can result in an unstable model when the input data distribution is significantly different from the one what used during the training.

3.3.1.2 Nonlinear state-selection

It is possible to build more compact PNLSS models using the nonlinear distortion information of the BLA. In general, not every resonance (state) is highly nonlinear, therefore it is not necessary

(or meaningful) to include these (nearly) linear states in the nonlinear part of the model given in (7).

This technique nonlinear state-selection technique results in a significant model order reduction that will improve the overall computational complexity and stability of models.

3.3.2 Nonlinear State-Space Neural Networks

3.3.2.1 Generic Nonlinear State-Space Neural Networks

An alternative and more generic way of expanding the nonlinear terms in (6) is the use of state-space neural networks (SSNN). The proposed SNNN is defined as

$$\begin{cases} x(t+1) = Ax(t) + Bu(t) + W_x g_x\left(V_x{}^T \begin{bmatrix} x(t) \\ u(t) \end{bmatrix} + b_{WVx}\right) + b_x \\ \quad y(t) = Cx(t) + Du(t) + W_y g_y\left(V_y{}^T \begin{bmatrix} x(t) \\ u(t) \end{bmatrix} + b_{WVy}\right) + b_y \end{cases} \tag{8}$$

where g represents a standard nonlinear activation function (such as hyperbolic tangent transfer function) with n_n neurons. $W_x \in \mathbb{R}^{n \times n_n}, V_x \in \mathbb{R}^{(n_i+n) \times n_n}$, $W_y \in \mathbb{R}^{n_o \times n_n}, V_x \in \mathbb{R}^{(n_i+n) \times n_n}$ are the weights, $b_{WVx} \in \mathbb{R}$, $b_x \in \mathbb{R}, b_{WVy} \in \mathbb{R}, b_y \in \mathbb{R}$ are the biases (offsets) . This formulation can be seen as a type of (shallow) recurrent neural network, referred to as a state-space neural network (SSNN). In our implementations, the weights in (8) are initialized randomly, and biases are set to zero initial values as suggested by [23].

The main advantage of using SSNN over deep neural networks that is SSNN results in more compact models leading to a substantial model reduction. Compared to PNLSS it offers more robustness for unforeseen input distributions, however, it offers much less interpretability.

3.3.2.2 Decoupled state-space models

The decoupled model structure is a special, single-hidden layer neural network where the activation functions are tailored to fit the data. The term decoupling comes from the fact that the technique was originally developed to decouple high dimensional functions, such as E_ζ and F_η terms in (7) into univariate terms as illustrated in Figure 4.

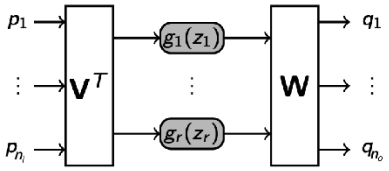

Figure 4. Graphical illustration of the decoupled structure.

The advantage of the decoupled structure is that the univariate functions can easily be visualized hence increasing the explainability of the model. The proposed state-space model is defined as (8) but with tailored activation functions. This means that g_x and g_y matrices will contain r univariate activaton functions (branches, or number of neurons in machine learning terms) that will be also estimated. Typically, in structural testing, the excitation and the output signals have zero mean values and such that the bias terms in (8) can be neglected further reducing the number of parameters.

4 THE GVT

4.1 Description of the measurement

This section provides a brief overview of the GVT measurement of a battery-operated small aircraft see (see Figure 5). The eFusion aircraft is a two-seat, all-electric, low-wing monoplane, based on a piston engine variant. The light sport aircraft has a symmetric wing profile, a titanium firewall, and a center section made of chrome molybdenum alloys. The fuselage is attached with a non-retractable tricycle landing gear. It has a length of 6.7 m, height of 2.4 m, and a wingspan of 8.3 m including winglet, whereas the wing area is 10.59 m². The aircraft is powered by a 60 kW electric drive system. The electric propulsion system including motor and batteries is designed by Siemens. The aircraft has an endurance of approximately one hour. The aircraft has an empty weight of 410 kg and a maximum take-off weight of 600kg. It requires a landing roll from 150 m to 200 m.

Figure 5: The eFusion battery-operated small aircraft

The measurement setup consists of 2 shakers–2 force cells (placed under the wings), and various 91 acceleration channels. The shaker reference (voltage) signals are random phase (odd) multisine signals. The sampling frequency is 200 Hz. The period length is 1024 resulting in a frequency resolution of 0.1953 Hz. The smallest excited frequency is 1.1719 Hz, the highest excited frequency is 50.7813 Hz. There are 7 different multisine realizations. Each multisine realization is repeated 3 times. The considered GVT experiment has been executed at two different excitation levels. At low-level excitation the shaker generates a broadband 2 N RMS excitation (with a measured SNR of 32 dB). At high-level excitation the excitation RMS is 10 N (with an SNR of 33 dB). The detailed modal analysis results of this GVT can be found in [8].

4.2 FRM analysis

Figure 6 shows the FRM at the driving points. Even though the high-level excitation is only 13 dB higher than the low-level excitation, it can be clearly observed that FRFs at different levels differ a lot from each other. This clearly indicated the presence of nonlinearities. However, for a given level of excitation, a novice user is not able to determine if there are nonlinearities present. Using the BLA framework we can directly estimate the noise and nonlinearity distortions.

For instance, at low-level, the first resonance (around 3 Hz, a rigid body mode) has an SNR of 30 dB and an SNLR (signal-to-nonlinearity ratio) of 40 dB. This means that at this resonance the main error source is the noise. At high level of excitation, the SNLR of this mode is around 28 dB, so at higher excitation level this rigid body mode behaves nonlinearly (what is to be expected).

Looking at the largest resonance (4th resonance at around 12 Hz, the first bending mode) one can conclude that at this resonance the dominant error source is the nonlinearity at all excitation levels. This kind of extra information would have been impossible to derive from the classical H_1 estimation framework. The detailed BLA results can be found in [7].

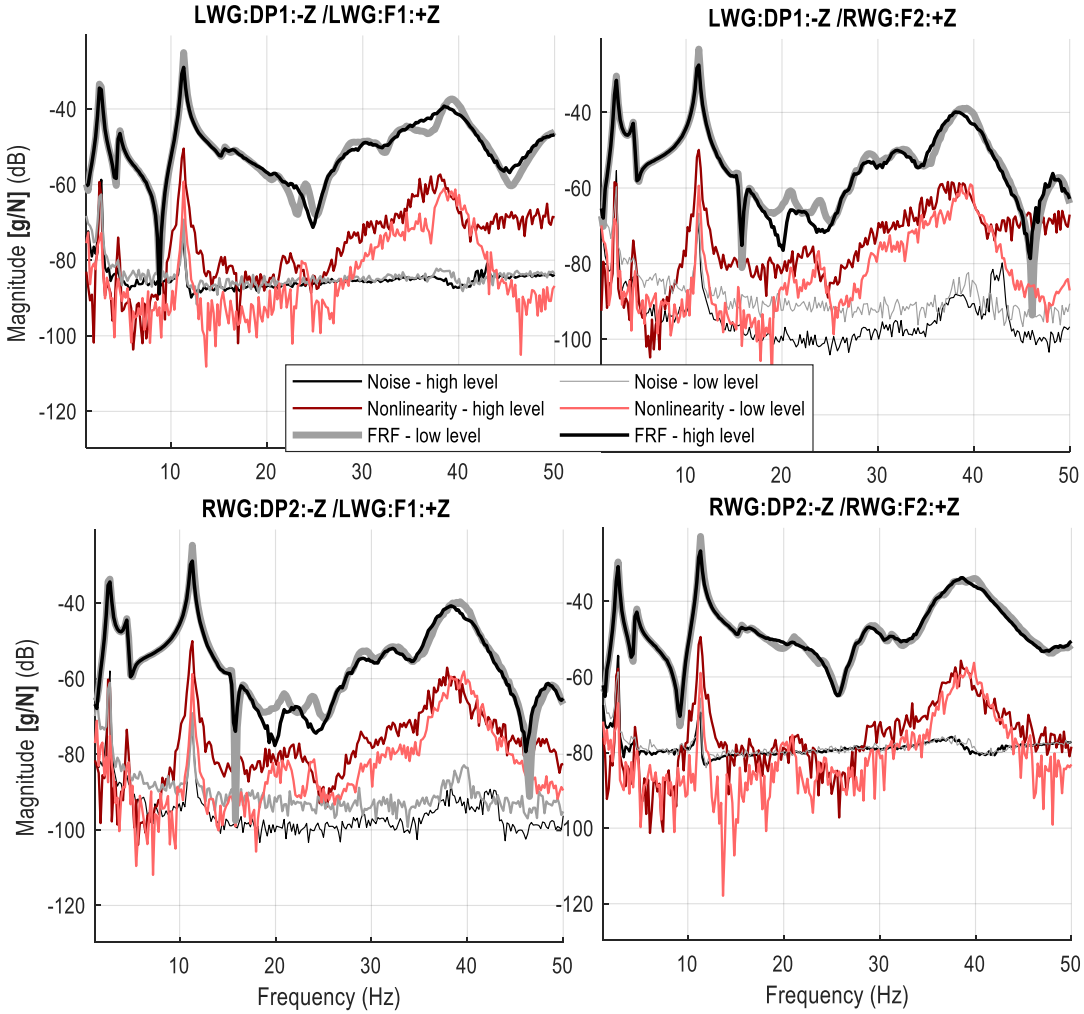

Figure 6: Noise and nonlinearity levels at with respect to one measurement block at low and high level of excitation.

5 THE MODELING RESULTS

In this section we provide a step-by-step description of the suggested nonlinear modeling approach.

5.1 The datasets

From each realization, only the steady-state periods are used, averaged (to reduce the noise and the computational needs) and the resulting data are split into three parts:

- Estimation dataset: 4-4 realizations from low- and high-levels of excitation are used to build the models,
- Validation datasets: 2-2 realizations from low- and high-levels of excitation are used to keep the model complexity under control,
- Test datasets: 1-1 realizations from low- and high-levels of excitation are used to compare different modeling approaches on a completely independent dataset.

The main metric used for comparison is the relative root mean squared error (rrmse) that is calculated in the time domain as:

$$\text{rrmse} = rms(\,(\hat{y} - y_{measured}))/rms(y_{measured} - mean(y_{measured})) \tag{9}$$

where $\hat{y}$ is a modeled output test signal and $y_{measured}$ is the measured output test signal. This rrmse will be calculated for both for low- and high-level data independently.

For data-driven modeling purposes, we only consider the flexible modes thus we exclude the rigid body modes – everything up to 8.5 Hz (this relatively high frequency is due to high flexibility and the light weight of the aircraft). All modeling results presented here are out-of-the-box solutions: no manual, fine tuning is applied. Table 1 shows the detailed fitting results.

5.2 FRF models

The first models to be assessed are the nonparametric FRM models. As expected, each FRM performs best on the level where it has been built.

From the FRF BLA distortion analysis the SNR and SNLR levels can be estimated. The SNLR/SNR levels provide a (rough) indication of the lower bounds of modeling error using a linear/nonlinear framework.

To establish some baseline number, the most distorted FRM channel is taken (the transfer between right wing acceleration and left wing excitation). The averaged SNLR level estimates for low-level is 27 dB, at high-level it is 20 dB. These values correspond to rrmse levels of 0.05 at low-level and 0.10 at high-level. The averaged SNR levels are 22 dB at low-level, corresponding to an rrmse of 0.08, and 21 dB at high-level corresponding to an rrmse of 0.09. It can be clearly concluded that at the low-level of excitation, the dominant error source is due to noise, at high-level the nonlinearities. These rrmse values give a weak indication of the lower bounds of the error.

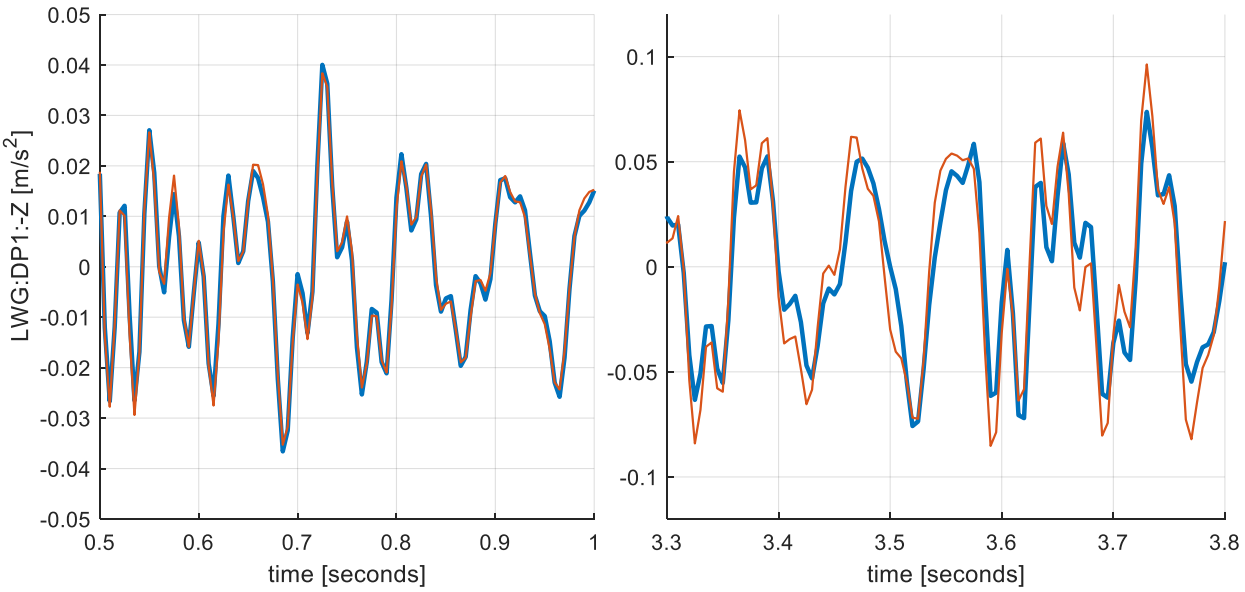

Figure 7: Output of the low-level BLA FRM model (red line) is compared to the measurement (blue line) on a segment of the left-wing acceleration test data. Left: low-level. Right: high-level.

5.3 SS models

As our experience shows, the best performance can be obtained when nonlinear models are initialized with a linear model trained on the most linear data, low-level experiments are considered here. All nonlinear models are initialized with the help of this SS BLA model.

As a second step, different parametric SS models are built based on the low-level nonparametric BLA FRM estimates. To determine the best model order (i.e. number of states), a cross-validation model-order scanning method is used between orders 1 and 30.

The overview of the model order scanning results, obtained on the validation dataset (which was not used for training), can be seen in Figure 8. The selected model order is 21 (states). This model order contains 529 parameters. Similar linear modeling error level can be observed with 8 states, however, this model would cover only a few (significant) modes. The main advantage of the proposed SS building technique that we obtain the modal SS representation what can be used – in combination with modal analysis techniques – determine what states represent which modes.

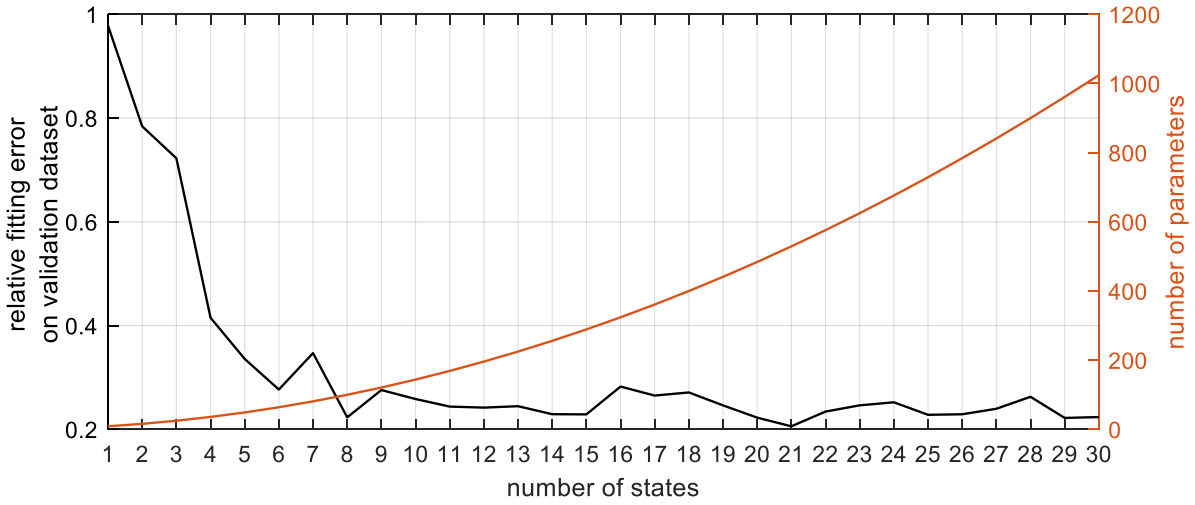

Figure 8: Parametric model fitting based on BLA FRM. State-space models are trained on the estimation dataset. Absolute rms errors are calculated on the validation datasets.

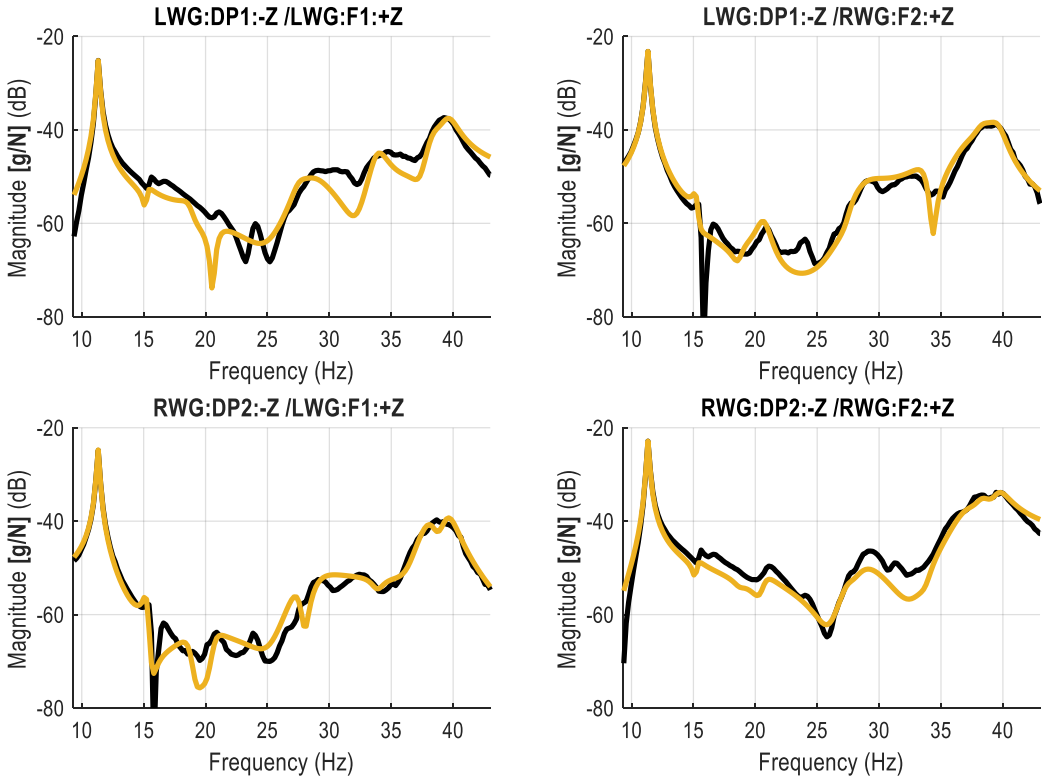

Figure 9: State-space models of order 21 estimated on the BLA FRM. Black lines represent the BLA FRFs, the orange lines represent the SS model.

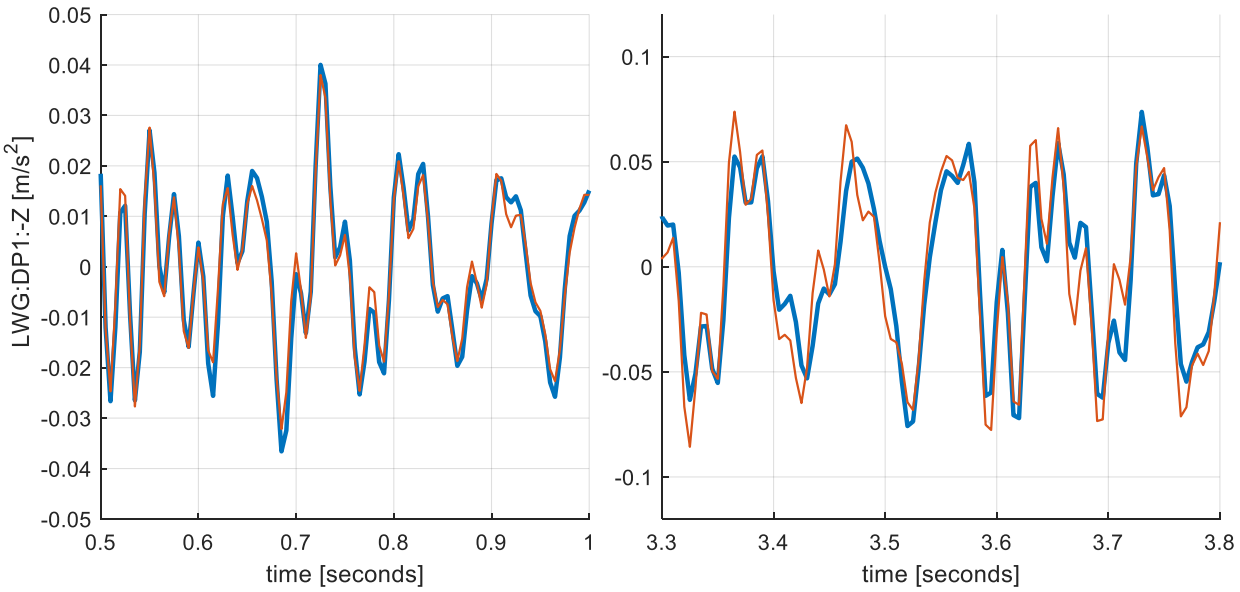

Figure 10: Output of the BLA SS model (red line) is compared to the measurement (blue line) on a segment of the left-wing acceleration test data. Left: low-level. Right: high-level.

5.4 PNLSS models

5.4.1 Generic PNLSS models

To reduce the model complexity and the computational needs, only nonlinearities in the state equation (i.e., matrix E_ζ in (7)) are considered with 2nd and 3rd order multivariate (state and input) monomials. A classical, all cross terms included PNLSS model with 21 states and two inputs results in a total of 54625 parameters. Using the estimation dataset and activating the nonlinearities in the output equation (i.e., matrix F_η in (7)) would require more than 16 GiB RAM, therefore it was not considered. For a fair comparison, in the case of SSNN models, no nonlinear terms in the output equations will be considered.

Seeing the fitting results of Table 1, one might wonder why the performance of the PNLSS model is so low: the rrmse is reduced only by 0.11 from 0.41 to 0.3. This main reason is that the ratio of training data samples (8192) and number of parameters (54625) is very low (0.15). To obtain a unique solution, the ordinary least squares algorithms require a ratio higher than 1 [12].

5.4.2 PNLSS models with nonlinear state-selection

The question arises: is it necessary to use all auto- and cross-terms of the states in the nonlinear part of the NSS equations or is it sufficient to use a lower number of well-chosen states? Using the BLA distortion information, one can directly estimate the significance of the nonlinear contributions per state, see Figure 6.

If we use only 2 nonlinear states at around 11 Hz (i.e., the first wing bending mode) we have good fitting results with an rrmse of 0.15. at a very low computational price of only 14 extra parameters on the top of the 529 SS model parameters. With 6 nonlinear states at around 11, 20, 40 Hz (first wind bending mode, the first horizontal tail bending mode, mixed torsional-bending mode) most of the nonlinear distortions are covered resulting in substantial improvement compared to the SS model resulting an rrmse increase from 0.41 rrmse to 0.13.

It is worth mentioning that one might use only the input terms in the nonlinear part of NSS. This results in lower rrmse fit (but it is factor 2 improvement compared to the BLA SS). The main advantage of this form is that this representation can be used directly in already existing linear simulation and controller setups. One might simply extend the B matrix with the coefficient of E_ζ and u input vector with second and third powers of the input.

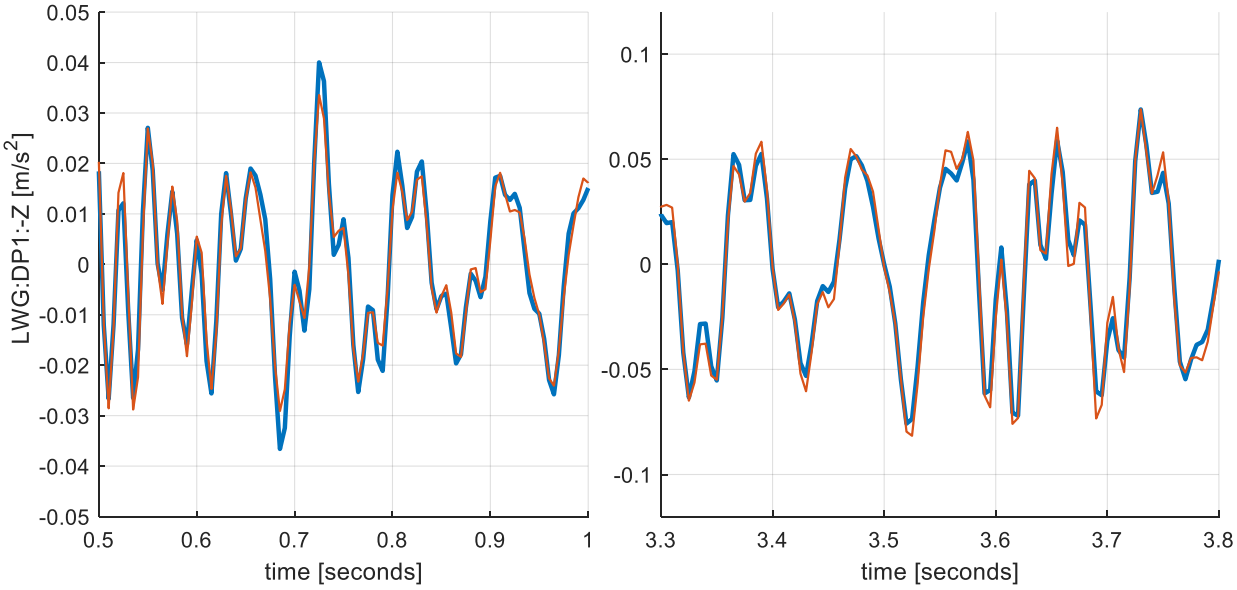

Figure 11: The output of the PNLSS model with 6 nonlinear states is compared to the measurement (blue line) on a segment of the left-wing acceleration test data. Left: low-level. Right: high-level.

5.5 SSNN models

5.5.1 Generic SSNN models

A model order scanning method has been applied with 1, 2, 5, 10, 20 neurons. Each model structure has 5 random initializations. This higher number of random realizations is needed because the unconstrained nonlinear optimization problem often results in a large spread of rrmse – unlike in the case of decoupled structure where most of the time the resulting models are nearly identical. The resulting models had a large random spread as per number of neurons and rrmse. The best result is found with 15 neurons using all states for the nonlinear part. This is because the latest implementation of the generic SSNN does not yet support the state variable selection. This model representation is completely black box as for the nonlinear terms, however, if the users are interested in a simple but efficient nonlinear method without the need for detailed interpretability, this method offers a good fit at a low computational (model complexity) cost.

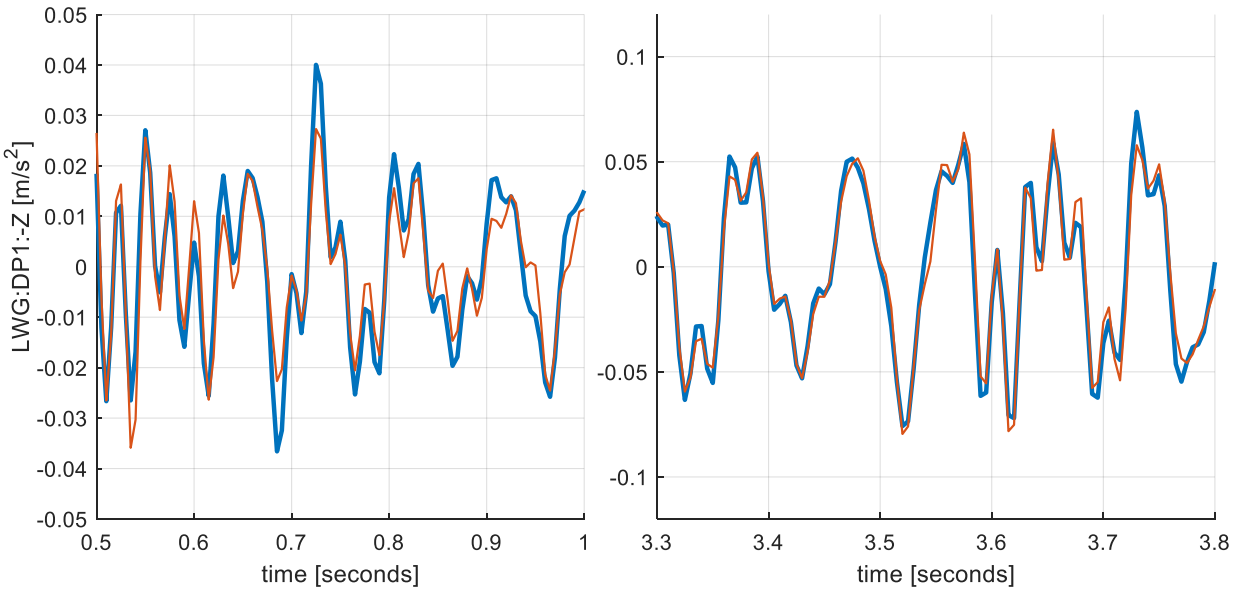

Figure 12: The output of the generic SSNN model with 15 neurons is compared to the measurement (blue line) on a segment of the left-wing acceleration test data. Left: low-level. Right: high-level.

5.5.2 Decoupled models

We tested the direct decoupling technique as well with 2 random realizations and a model order scanning between 1 and 5 branches. The fitting results are improved compared to the generic SSNN structure.

In the first modeling attempt, all states were considered, and the best model has been found with 1 branch (i.e., 1 custom activation function). In the second modeling attempt, when only the 6 selected states are considered for the nonlinear model part, then a solution with 3 branches has been found. It is important to mention that there was so significant difference between the models in terms of rrmse. It is because in the case of the decoupled model structure, we have very limited number of parameters: per branch, for each state there are two variables (weights in terms of neural networks) assigned, and for each input there is one variable assigned. This means that including all states or only a few selected states in the nonlinear extension part does not significantly change the model complexity. For determining the activation function (the branch) we use a 4th order polynomial fit (i.e., 5 parameters) for smooth function estimation. The estimated three branches (activation functions) are shown in Figure 13. The odd shapes of activation function are not surprising. In general, odd nonlinearities are responsible for moving resonance frequencies (it is the so-called hardening or softening stiffness nonlinearity effect).

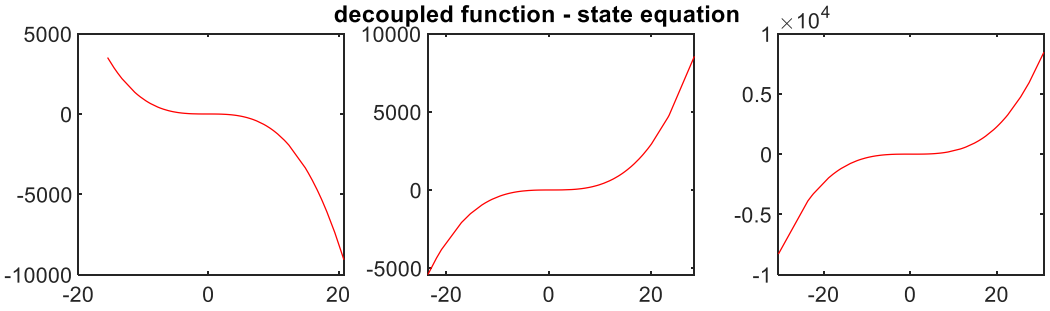

Figure 13: Illustration of three branches (activation functions).

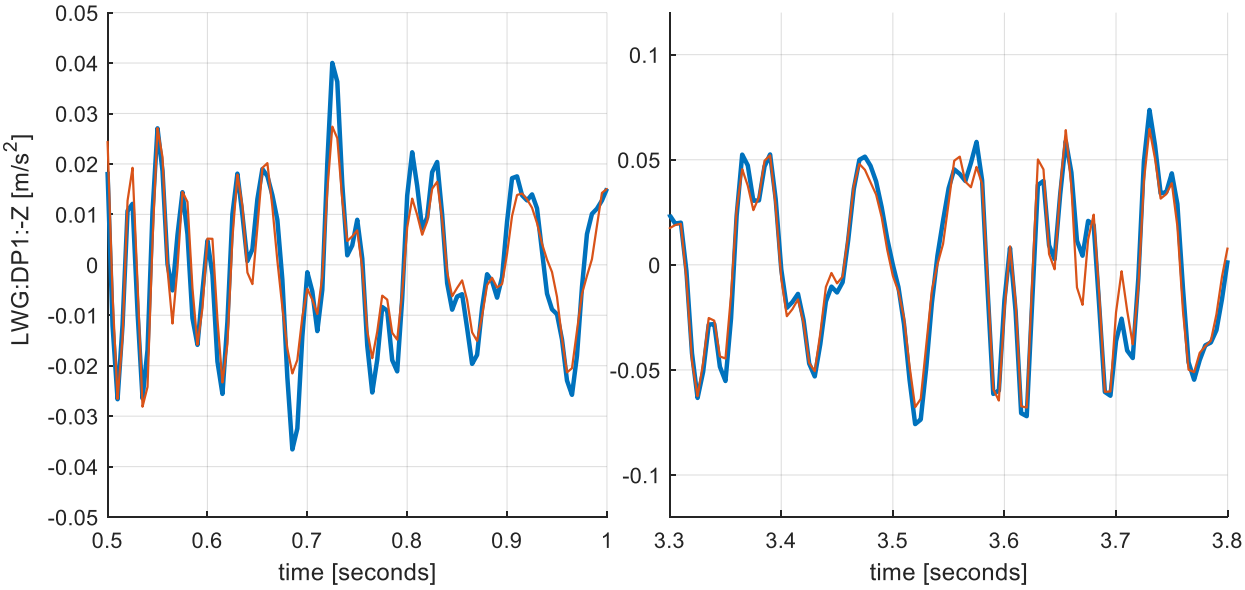

Figure 14: The output of the decoupled model with 6 nonlinear states and three branches is compared to the measurement (blue line) on a segment of the left-wing acceleration test data. Left: low-level. Right: high-level.

5.6 Summary

An overview of the best obtained modeling results is shown in Table 1. As the nonparametric analysis shows, the MIMO GVT measurement is nonlinear. This means that using a simple linear model may result in unacceptable accuracy. To build SS models we used an FRM-based fitting technique because its robustness and simplicity. We considered an SS model built on the low-level data using 21 states.

The classical PNLSS models come with a hefty price tag: the tuning time and the memory needs are excessive due to the extremely high number of nonlinear parameter terms (54096). The performance of the full PNLSS models can be further improved using the nonlinear state-space selection method resulting in a drastic decrease of number of nonlinear parameters (936 in case of 6 nonlinear states, and 23 in case of inputs only).

A more time-saving option can be using the decoupled model structures or the generic SSNN models. The obtained results provide an excellent balance between the number of parameters computational time and the performance. The main drawback of the generic SSNN is that the model interpretability is somewhat limited.

The results can be further optimized using 1) more data for tunning, 2) more optimization steps of other optimization routine, 3) fine tuning the model structure, and in case of neural network models 4) using more random realizations.

Table 1. Overview of the modeling results.

Model	Relative rms error on test data				Computational time*	Number of parameters	Memory need of the tuning method*
	Low-level	High-level	Mean	Un-weighted mean			
low-level BLA FRM	0.11	0.43	0.27	0.41	<1 sec	174	< 1 GiB
high-level BLA FRM	0.48	0.28	0.38	0.30	<1 sec	174	< 1 GiB
BLA SS of 21 states	0.19	0.43	0.31	0.41	< 1 minute	529	< 1 GiB
PNLSS with 21 NL states	0.18	0.31	0.25	0.30	< 1 day	529 +54096	< 16 GiB
PNLSS with 2 NL states	0.22	0.14	0.18	0.15	< 1 hour	529+14	< 4 GiB
PNLSS with 6 NL states	0.16	0.09	0.13	0.12	< 2 hours	529+936	< 4 GiB
PNLSS with 6 NL states - inputs only	0.24	0.20	0.22	0.21	< 1 hour	529+42	< 4 GiB
SNNN 15 with neurons	0.22	0.20	0.21	0.20	< 10 minutes whole process: < 1 hour	529+698	< 4 GiB
Decoupled model 21 NL states1 branch	0.23	0.17	0.20	0.18	< 10 minutes entire process: < 1 hour	529+49	< 4 GiB
Decoupled model 6 NL states, 3 branches	0.28	0.18	0.23	0.19	< 5 minutes whole process: < 0.5 hour	529+57	< 4 GiB

* exact figures depend on the hardware and software implementations (a low-cost laptop has been used for the model fitting).

6 CONCLUSIONS

Nonlinear black-box modeling of complex real-world nonlinear systems is computationally demanding as a high number of model parameters is needed. This generally results in a loss of interpretability as well.

In this study, we presented modeling approaches aimed at addressing these challenges. The first approach extends the classical PNLSS framework with a nonlinear-state selection process, leveraging insights from signal-to-noise and signal-to-nonlinearity ratios derived from the BLA framework. The second approach utilizes SSNN either with tailored activation functions or with generic activation functions. We show how both strategies allow to maintain or even improve the interpretability of nonlinear models while keeping the model order under control.

The proposed nonlinear modeling framework is illustrated on ground vibration testing of the Magnus eFusion light sports aircraft.

ACKNOWLEDGEMENT

This work was funded by the VLAIO AVIATOR project under grant number HBC.2022.0800 and SRP60 of the Vrije Universiteit Brussel.

REFERENCES

[1] P. Z. Csurcsia, J. Decuyper, B. Renczes, M. Runacres and T. D. Troyer, "Reducing black-box nonlinear state-space models: A real-life case study," *Mechanical Systems and Signal Processing,* vol. 211, p. 111230, 2024.

[2] L. Lauwers, J. Schoukens, R. Pintelon and M. Enqvist, "Nonlinear Structure Analysis Using the Best Linear," in *Proceedings of International Conference on Noise and Vibration Engineering*, Leuven, 2006.

[3] J. Schoukens and R. Pintelon, "Study of the Variance of Parametric Estimates of the Best Linear Approximation of Nonlinear Systems," *IEEE Transactions on Instrumentation and Measurement,* vol. 59, no. 12, pp. 3156-3167, 2010.

[4] J. Paduart, Identification of nonlinear systems using Polynomial Nonlinear State Space models, Belgium: PhD thesis, 2008.

[5] M. Elkafafy, P. Z. Csurcsia, B. Cornelis, E. Risaliti and K. Janssens, "Machine learning and system identification for the estimation of data-driven models: An experimental case study illustrated on a tire-suspension system," in *Proceedings of ISMA 2020 - International Conference on Noise and Vibration Engineering and USD 2020 - International Conference on Uncertainty in Structural Dynamics, 2020, pp. 3287–3301*.

[6] J. Decuyper, K. Tiels, M. Runacres, J. Schoukens, "Retrieving highly structured models starting from black-box nonlinear state-space models using polynomial decoupling," *Mechanical Systems and Signal Processing,* vol. 146, 2021.

[7] P. Z. Csurcsia, B. Peeters, J. Schoukens, "The Best Linear Approximation of MIMO Systems: First Results on Simplified Nonlinearity Assessment," in *Nonlinear Structures and Systems, Volume 1. Conference Proceedings of the Society for Experimental Mechanics Series. Springer, Cham.*, 2020.

[8] E. Di Lorenzo, U. Musella, S. Vettori, R. Hallez, R. Debille, B. Peeters, W. Flynn and P. Z. Csurcsia, "Structural dynamics assessment on a full-electric aircraft: Ground vibration testing and in-flight measurements," in *International Forum on Aeroelasticity and Structural Dynamics 2019, IFASD 2019*.

[9] P. Z. Csurcsia, B. Peeters, J. Schoukens, T. De Troyer, "Simplified Analysis for Multiple Input Systems: A Toolbox Study Illustrated on F-16 Measurements," *Vibration,* vol. 3, no. 2, pp. 70-84, 2020.

[10] R. Pintelon, J. Schoukens, System Identification: A Frequency Domain Approach, 2nd ed., New Jersey: Wiley-IEEE Press, ISBN: 978-0470640371, 2012.

[11] P. Z. Csurcsia and J. Lataire, "Nonparametric Estimation of Time-variant Systems Using 2D Regularization," *IEEE Transactions on Instrumentation & Measurement,* vol. 65, no. 5, pp. 1259-1270, 2016.

[12] J. Schoukens, R. Pintelon, Y. Rolain, Mastering System Identification in 100 exercises, New Jersey: John Wiley & Sons, ISBN: 978047093698, 2012.

[13] W. Heylen, P. Sas, Modal Analysis Theory and Testing, Leuven: Lirias, 2005.

[14] T. Dobrowiecki, J. Schoukens, P. Guillaume, "Optimized excitation signals for MIMO frequency function measurements," *IEEE Transactions on Instrumentation and Measurements,,* vol. 55, pp. 2072-2079, 2006.

[15] M. Blanco, P. Z. Csurcsia, B. Peeters, K. Janssens and W. Desmet, "Nonlinearity assessment of MIMO electroacoustic systems on direct field environmental acoustic testing," *Proceedings of ISMA 2018 - International Conference on Noise and Vibration Engineering and USD 2018 - International Conference on Uncertainty in Structural Dynamics,* p. 457–471, 2018.

[16] B. Cornelis, A. Toso, W. Verpoest, B. Peeters, "Improved MIMO FRF estimation and model updating for robust Time Waveform Replication on durability test rigs," in *International Conference on Noise and Vibration Engineering*, Leuven, 2014.

[17] P. Z. Csurcsia, B. Peeters, J. Schoukens, "User-friendly nonlinear nonparametric estimation framework for vibro-acoustic industrial measurements with multiple inputs," *Mechanical Systems and Signal Processing,* vol. 145, 2020.

[18] P. Z. Csurcsia, "MUMI: Multisine for multiple input systems: A user-friendly excitation toolbox for physical systems," *Software Impacts,* vol. 11, p. 100192, 2022.

[19] P. Z. Csurcsia, B. Peeters and J. Schoukens, "The best linear approximation of MIMO systems: Simplified nonlinearity assessment using a toolbox," *Proceedings of ISMA 2020 - International Conference on Noise and Vibration Engineering and USD 2020 - International Conference on Uncertainty in Structural Dynamics,* p. 2239–2252, 2020.

[20] P. Z. Csurcsia, "LPRM: A user-friendly iteration-free combined Local Polynomial and Rational Method toolbox for measurements of multiple input systems," *Software Impacts,* vol. 12, p. 100238, 2012.

[21] McKelvey, T., Akçay, H., & Ljung, L., "Subspace-based multivariable system identication from frequency response data," *EEE Transactions on Automatic Control,* vol. 41, pp. 960-979, 1996.

[22] P. Van Overschee and B. De Moor, Subspace Identification of Linear Systems: Theory, Implementation, Applications, Springer Publishing, 1996.

[23] M. Schoukens, "Improved Initialization of State-Space Artificial Neural Networks," *2021 European Control Conference (ECC),* pp. 1913-1918, 2021.

COPYRIGHT STATEMENT